Methodology development of electrical conductivity measurements for non-ferrous slags

Pieter-Jan Boeykens[1], Roman Starykh[2], Maksym Shevchenko[3], Lennart Scheunis[4], Amy Van den Bulck[5], Evgueni Jak[6]; Inge Bellemans[7], Kim Verbeken[8]

1. PhD Candidate, Ghent University, Ghent Oost-Vlaanderen Belgium.
   Pieterjan.boeykens@ugent.be
2. Research Fellow, University of Queensland, Brisbane Queensland Australia.
   r.starykh@uq.edu.au
3. Research Fellow, University of Queensland, Brisbane Queensland Australia.
   m.shevchenko@uq.edu.au
4. Senior Scientist, Umicore N.V., Olen Antwerpen Belgium.
   lennart.scheunis@eu.umicore.com
5. Scientist, Umicore N.V., Olen Antwerpen Belgium.
   amy.vandenbulck@eu.umicore.com
6. Full Professor, University of Queensland, Brisbane Queensland Australia.
   e.jak@uq.edu.au
7. Assistant Professor, Ghent University, Ghent Oost-Vlaanderen Belgium.
   inge.bellemans@ugent.be
8. Full Professor, Ghent University, Ghent Oost-Vlaanderen Belgium.
   kim.verbeken@ugent.be

Keywords: Pyrometallurgy, non-ferrous slags, electrical conductivity, iron oxidation state

ABSTRACT

As a result of the globally increasing consumer use of electronic devices, it is expected that pressure will increase on the supply chain of precious metals. Hence, recycling of these electronics becomes increasingly important, as well as optimizing the current processes. One major issue in metallurgical processes is the amount of metal that is lost into the slag. This metal loss is inherent to the production process and therefore, additional processing steps such as slag cleaning may be required. Slag cleaning can be done in electrical resistance furnaces where heat is produced using the Joule effect, making the slag's electrical conductivity an important operating parameter. Since slags are ionic liquids, the electrical conduction happens via the movement of ions which is called ionic conductivity. However, within the presence of transition metal oxides, a second mechanism of conductivity occurs as electrons are able to hop from one transition state to another, which is known as electronic conductivity. As 'FeO' is a common slag component in the non-ferrous pyrometallurgical industry, both mechanisms are present, but their proportions vary with the respective amounts of the two forms of the multi-valent ions and hence, with the oxygen partial pressure. The goal of the present study is to develop an experimental setup and methodology for measuring the electrical conductivity of synthetic SiO_2 – CaO – $AlO_{1.5}$ – 'FeO' slags at various oxygen partial pressures.

INTRODUCTION

One of the major current challenges within the metallurgical industry is the reduction of CO_2 emissions or so called decarbonization. To achieve decarbonization, the typical paths being explored are the use of green hydrogen as alternative for fossil based reductants and/or the electrification of production processes (Dalvi, 2023). In addition to decarbonization, reduction of metal losses during primary production and recycling should also be taken into account to optimise resource efficiency. During pyrometallurgical processing, metal is frequently lost to the slag (metal oxide) phase as either a dissolved oxide or entrained droplets (Bellemans *et al.*, 2018). One way to target both challenges is the use of submerged electric arc furnaces which operate as a decantation furnace to allow metal droplets from the slag to settle and be recovered while heat is generated via the conversion of electricity using the slag's resistance (Joule heating) (Friedrich *et al.*, 2018). As a result, the modelling, dimensioning and operating of these furnaces require knowledge on the electrical conductivity of the used slag (Karalis *et al.*, 2016).

The present study focusses on silicate slags containing CaO, $AlO_{1.5}$[1] and 'FeO'[2] and thus current will be carried via both ionic and electronic conduction. The ionic mechanism involves the movement of cations (Ca^{2+}, Fe^{2+}) throughout the (alumino)silicate network (Mills *et al.*, 2013). The main factors affecting the ionic conductivity are the amount of network forming oxides (SiO_2, $AlO_{1.5}$[3]), the size of the mobile/network breaking cations and their valence. Electronic conduction within slags requires the presence of transition metal oxides in different oxidation states which allows electrons to hop from one oxidation state to the other (Barati and Coley, 2006a). As this second mechanism is highly dependent on the iron oxidation state, the electrical conductivity of 'FeO'-containing slags is rather sensitive to the applied gas atmosphere, i.e. the oxygen partial pressure (Hundermark, 2003; Barati and Coley, 2006a).

In order to obtain more insight in both mechanisms and to construct a predictive model, a lot of accurate data on both contributions is required. This in turn demands experimental techniques to distinguish between both contributions. One such experimental method is stepped potential chronoamperometry which was proposed by Fried et al. for BaO-'TiO_2' slags (Fried, Rhoads and Sadoway, 2001). This technique was applied by Barati and Coley (Barati and Coley, 2006a) for SiO_2 – CaO – 'FeO' slags and recently by Liu et al. on the SiO_2 – CaO – $AlO_{1.5}$ – 'FeO' system (Liu, Zhang and Chou, 2015; J. H. Liu *et al.*, 2016; Liu *et al.*, 2018). In each study, the oxygen partial pressure (p_{O2}) was varied to study its effect on the slag's electrical conductivity.

However, neither study verified the slag's chemical composition or microstructure after the experiment. In addition, the influence of the crucible was also not reported in any studies. For the study of Barati and Coley, zirconia (ZrO_2) crucibles were used and thus there could be an influence of zirconia dissolution within the slag. Liu et al. used Pt crucibles of which is known that they can react with FeO at sufficiently low p_{O2} values which results in the uptake of Fe in the Pt crucible (Schupsky *et al.*, 2020). Also, it is unclear for both studies whether they targeted a similar bath volume/bath height for each experiment and between the high temperature experiments and room temperature calibrations. Thus, in order to further improve the methodology of high temperature conductivity experiments, an experimental setup was developed that allows quenching of the slag and crucible after each experiment for microstructural analysis. The aim of the present paper is, on the one hand, to verify that our electrical conductivity apparatus provides reliable experimental data and, on the other hand, to further contribute to the experimental methodology within the field.

[1] The authors prefer the use of $AlO_{1.5}$ over Al_2O_3 for the alumina content in the slag system as this gives an easier visualization of the amount of cations in the slag, which are the main contributors to the ionic conductivity.
[2] 'FeO' is used throughout the text as a representation of iron oxide regardless of the iron oxidation state.
[3] $AlO_{1.5}$ is technically an amphoteric oxide, meaning that it can both have a network forming and network breaking role in the slag.

METHODOLOGY

Electrical conductivity measurements

A detailed overview of general electrical conductivity measurements by the present authors was already published before (Boeykens *et al.*, 2023b) and as such a summary of the measurement technique is given. The electrical conductivity of a material is derived from the resistance according to equation 1) in which σ_{tot} is the total conductivity ($S \cdot cm^{-1}$), R is the measured resistance (Ω), l is the length of the current path (cm) and A is the cross-section of the current path (cm^2). The length l and the area A are typically grouped together in a geometric constant G which is known as the cell constant (cm^{-1}). For a solid material, the geometry of the sample can be measured and thus, the cell constant is easily determined. However, as a slag is a liquid/suspension, it needs to be put in a container and electrodes have to be submerged into the liquid. As a result, the current can travel throughout the entire volume of the container and therefore, a calibration is necessary to take into account the geometry of the current path. Typically, calibration procedures are carried out with aqueous solutions of which the conductivity is well known. During the calibration, the temperature is also carefully recorded, as the electrical conductivity has an Arrhenian temperature dependency as shown in equation *2*) in which E_a is the activation energy ($J \cdot mol^{-1}$), R the universal gas constant ($J \cdot mol^{-1} \cdot K^{-1}$), T the temperature (K) and σ_0 a pre-exponential factor ($S \cdot cm^{-1}$).

$$\sigma_{tot} = \frac{l}{A} * \frac{1}{R} = \frac{G}{R} \quad 1)$$

$$\sigma(T) = \sigma_0 exp\left(\frac{-E_a}{RT}\right) \quad 2)$$

Second, a slag is an ionic liquid and therefore, the current is (partially) carried via the movement of ions. As such, direct current (DC) resistance measurements are impossible due to polarization of the ions at the electrodes which blocks the current (Fried, Rhoads and Sadoway, 2001). Therefore, an alternating current (AC) needs to be applied and the slag's resistance/conductivity needs to be derived from the impedance Z (Ω). As the current is applied as a sine wave with a certain frequency f (Hz), capacitive and inductive responses of the melt/measurement set-up are measured as well and thus, the impedance is divided in a real Z_{real} (Ω) and imaginary part Z_{im} (Ω), as shown in equation 3), which are both frequency dependent (Bard and Faulkner, 2001).

$$Z_{tot}(f) = Z_{real}(f) + j * Z_{im}(f) \quad 3)$$

To isolate the resistance corresponding to the slag's electrical conductivity, a frequency sweep is carried out to locate a frequency f_0 for which $Z_{im} = 0$. Typically though, a region of frequencies is found where the impedance is frequency independent and $Z_{real}(f) = Z_{real}(f_0)$.

Third, the aim of the current work is to measure the conductivity of '$FeO^{'}$'-containing slags for which it is known that they exhibit both ionic and electronic conduction (Hundermark, 2003; Barati and Coley, 2006a, 2006b; Liu, Zhang and Chou, 2015; J. H. Liu *et al.*, 2016; Liu *et al.*, 2018). From AC impedance measurements, the total conductivity of the slag can be derived which includes the contribution of both ions and electrons as charge carriers. To measure the contribution of each charge carrier, Fried et al. (Fried, Rhoads and Sadoway, 2001) proposed a method to determine the electronic transference number t_e (-) from stepped potential chronoamperometry (SPC) measurements. In their work, they laid the theoretical foundations of this technique applied for a binary BaO – 'TiO_2' system. The SPC technique has since been used in several slags containing transition metals such as Fe, Mn and Ti (Barati and Coley, 2006a; Pomeroy *et al.*, 2012; Liu, Zhang and Chou, 2015; J. H. Liu *et al.*, 2016; Jun Hao Liu *et al.*, 2016; Liu, Zhang and Wang, 2017; Liu *et al.*, 2018; Martin-Treceno *et al.*, 2022; Boeykens *et al.*, 2023a).

The basic idea of SPC is that a small DC voltage is applied to the slag and that the responsive current is recorded as a function of time. If the applied voltage is sufficiently low so that no faradaic reactions occur, then polarization of the ions occurs and as a result ionic conduction will cease to happen at a certain time. On the contrary, electrons will continue to hop from one oxidation state to the other. The resulting current as a function of time will therefore have a current peak at the start and will decay to a stable, lower value. An example of such a voltage step and corresponding decaying current is provided in FIG - *1*. Assuming a homogeneous spread of the cations within the

slag before the voltage step, the initial current response or the current peak I_{peak} corresponds to both ions and electrons moving within the slag. Due to the current decay, after a sufficiently long time, only electrons will continue to pass on current and this corresponds to I_{∞}.

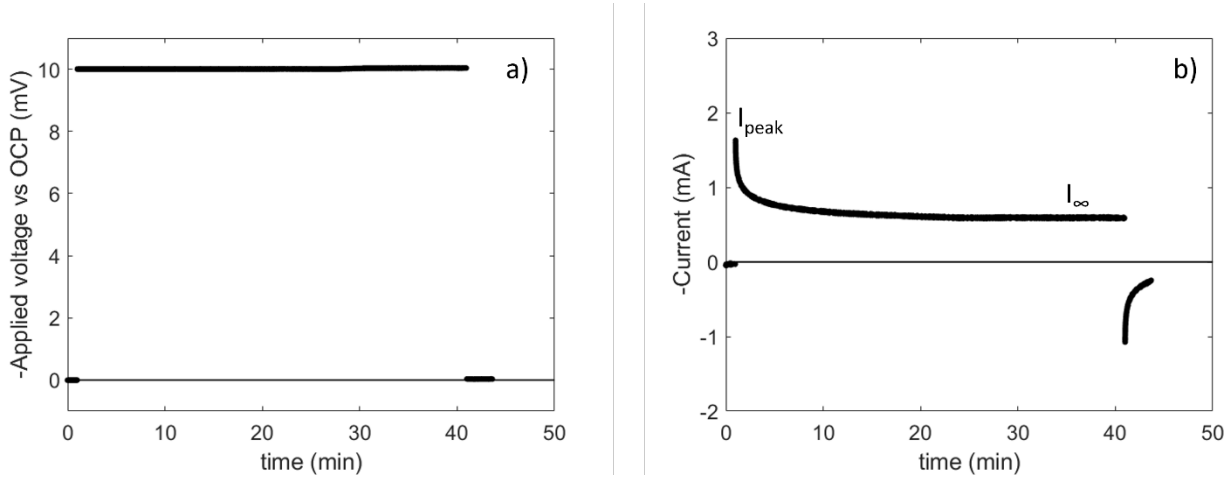

FIG - 1 a) Example of the applied voltage step versus open circuit potential (OCP) and b) example of the current response for stepped potential chronoamperometry (SPC).

The relative contribution of each charge carrier to the total current is denoted as the transference number. Thus, from the SPC measurement, the electronic transference number is equal to the ratio of the stable current over time, I_{∞}, over the initial peak current, I_{peak} as shown in equation *4*). Correspondingly, the ionic transference number t_i can be derived from t_e as the sum of both equals unity by definition (equation *5*)).

$$t_e = \frac{I_{\infty}}{I_{peak}} \quad 4)$$

$$t_i + t_e = 1 \quad 5)$$

The transference numbers can then be utilized to determine the ionic σ_i and electronic conductivity σ_e of the slag via multiplying the respective transference number with the total conductivity obtained from AC impedance measurements as given in equations *6*) and *7*). This is, however, on the assumption that the charge carriers are homogeneously distributed within the melt and that each charge carrier is similarly affected by the applied potential.

$$\sigma_i = t_i * \sigma_{tot} \quad 6)$$

$$\sigma_e = t_e * \sigma_{tot} \quad 7)$$

Electrical conductivity apparatus

Electrical conductivity measurements were performed in a high-temperature setup similar to the one developed and described in an earlier article (Zhao *et al.*, 2009). A schematic drawing of the apparatus is shown in FIG - 2. The setup can be divided into three parts: 1) A Pyrox vertical tube furnace (resistive heating up to 1650 °C) with a temperature controller, 2) a steel chamber at the top which houses three vertically moving platforms and the electrode holder and 3) a stainless steel guiding tube at the bottom of the furnace which is placed in a bucket containing water. Optionally, a stainless steel tip can be placed inside the bucket as well. The furnace was made gas-tight via sealing of the top steel chamber with a plastic window and via submerging the quench-guiding tube in the quenching water.

An alumina crucible was used to contain the slag and this crucible was positioned within the isothermal zone of the furnace via an alumina suspension tube which is connected to the suspension platform. To ensure the connection between the crucible and the suspension tube, both the crucible and the tube have four holes through which Pt – 13% Rh wires were inserted. The electrodes were

placed within an electrode holder on the electrode platform. A digital displacement sensor with a 90 mm stroke and 0.01 mm precision was placed on the movable electrode platform to monitor the movement of the electrodes. To quench the crucible from the furnace, two alumina plunger rods were positioned on the plunger platform inside the suspension tube so that they touch the top of the crucible. Via lifting up the suspension platform and keeping the plunger platform stationary, the plunger tubes push on the crucible which shears/breaks the Pt wires allowing the crucible to fall into the quenching water. When the stainless steel tip is placed inside the quenching water, the alumina crucible will shatter on impact. This causes direct contact between the hot slag (1310 °C) and the water (25 °C) to ensure fast quenching. This quenching procedure allows to freeze the sample microstructure at high temperature which subsequently can be analysed via microscopic techniques to verify the slag composition, the presence of any solids, etc. However, the quenching procedure with the stainless steel tip cannot provide information on the location and distribution of eventual solids within the slag. Therefore, some experiments were also carried out without the steel tip which allows the crucible to be quenched as a whole. A microscopic analysis was then carried out on the crucible cross-section instead.

The temperature of the furnace in the hot zone was calibrated using a type B thermocouple at different heights, while the oxygen partial pressure (p_{O2}) was controlled via controlling the ratio of (CO + Ar)/CO_2 gas inside the furnace. The ratio of both gas mixtures was adjusted to meet the desired target p_{O2} using a similar procedure as the small scale equilibrium experiments. A total flow rate of 1 l/min was used. To verify the current setup, three p_{O2} values were chosen: air (0.21 atm), 10^{-5} atm and $10^{-7.92}$ atm which correspond to Fe^{3+}/Fe_{tot} ratios of 0.89, 0.51 and 0.20, respectively, as predicted by FactSage (UQPY database (Evgueni *et al.*, 2022))

Given the high conductivity of 'FeO'-containing slags, a four-electrode setup was utilised to measure the electrical conductivity as this method omits the need for cable corrections and the potential errors associated with two-electrode set-ups (Boeykens *et al.*, 2023b). The electrodes were made of 25 mm long 1 mm diameter Pt – 30% Ir tips which were welded to a long thin (0.3 mm diameter) Pt – 30% Ir wire. The electrodes were sheathed into a single bore alumina tube (inner diameter = 1 mm). The tips were positioned 5 mm inside the alumina tube to fix their position. In addition, the position of the tubes with respect to each other was fixed via three ceramic spacers along the length of the alumina tubes. A detailed schematic of the electrode positions with respect to each other and the crucible is provided in FIG - 2. The thin wires were connected via electrical connectors to electrically isolated steel bolts which protrude the top steel chamber. As a result, alligator clips were clipped to these bolts to make the electrical connection between the Gamry 1010E Interface potentiostat and the electrodes. A potentiostat was utilised as both AC and DC measurements are needed to fully describe the electrical conductivity of 'FeO'-containing slags.

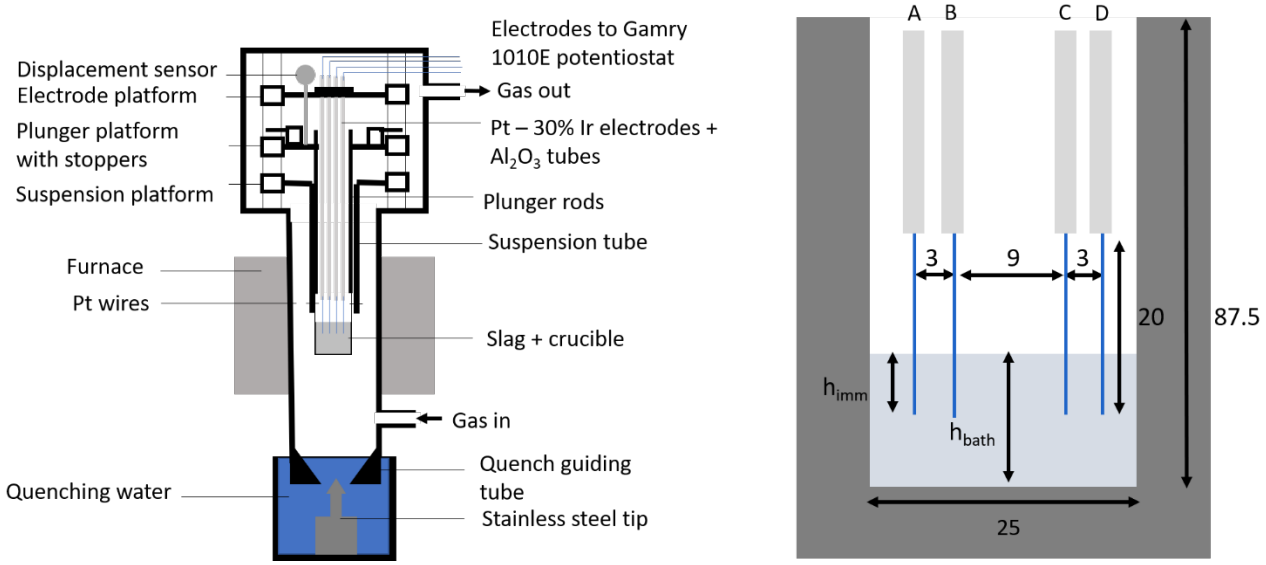

FIG - 2 Schematic overview of the high temperature electrical conductivity setup and detailed close-up of the electrode and crucible geometry. Dimensions are in mm.

Measurement procedure

Cell calibration

As mentioned earlier, the geometry of the current path or the cell constant G needs to be determined in order to convert resistances to electrical conductivities. As the cell constant is (strongly) dependent on the cell construction in terms of electrode geometry, electrode immersion depth, crucible material, solution, etc. (Gruener *et al.*, 1998; Schiefelbein *et al.*, 1998; Boeykens *et al.*, 2023b), the calibration was done as a function of the electrode immersion depth h_{imm} (3 mm – 15 mm) for different bath heights h_{bath} (21 mm, 23 mm, 25 mm and 27 mm). An aqueous 1 D (demal) KCl conductivity standard (111.3 mS/cm at 25 °C, Radiometer analytical) was chosen as the calibration liquid.

The bath surface was located via lowering the electrodes and simultaneously measuring the impedance. In air, the impedance was of the order kΩ/MΩ and strongly fluctuated, whereas when it touched the conductive liquid, the impedance dropped to an order of Ω and was stable. This process was done via a two-electrode configuration using multiple electrode combinations (A-B, A-C and A-D in FIG - *4*). The bath surface was set to be the displacement sensor reading for which all electrodes touched the bath surface. The electrodes were subsequently lowered to an immersion depth of 10 mm for calibration impedance measurements.

These measurements were done galvanostatically using an excitation current of 100 µA. For each experiment, a frequency sweep was first carried out at a 10 mm immersion depth to determine the frequency at which the solution's resistance can be extracted. The real impedance was found to be frequency independent between 10 kHz and 100 kHz at 10 mm insertion for different bath heights and calibration solutions. Thus, single frequency measurements were done at 20 kHz for 3 minutes. After the single frequency measurement, the electrode's position was changed to vary the immersion depth and the single frequency measurement at 20 kHz was repeated. During each measurement, the temperature was recorded using a type-K thermocouple next to the crucible. The temperature dependency of the conductivity standards was fitted to equation *2*) from data provided by the suppliers. From this fit, the electrical conductivity at the measured temperature was determined and multiplied by the measured real impedance at 20 kHz to obtain the cell constant G. The measured cell constant as a function of the immersion depth and bath is shown in FIG – 3.

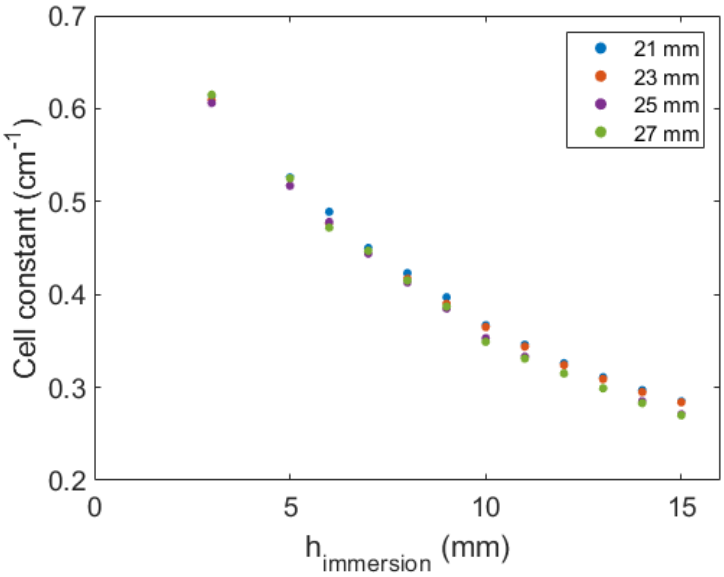

FIG - 3. Cell constant G (cm^{-1}) as a function of the electrode immersion depth h_{imm} (mm) for different bath heights.

High temperature measurements

For the high-temperature conductivity measurements, a bath height of 25 mm was desired. The amount of slag needed was calculated based on the density/molar volume model of Thibodeau et

al. (Thibodeau, Gheribi and Jung, 2016a, 2016c, 2016b). The slag mixture was prepared in two steps. First, a sinter of CaO – $AlO_{1.5}$ – SiO_2 (CAS) was prepared via mixing high-purity powders of $CaCO_3$ (99.9%), Al_2O_3 (99.7%) and crushed SiO_2 glass (99.999%) together to match the compositions in TABLE 1. Fe and Fe_2O_3 were added to create the predicted amount of FeO according to calculated via FactSage 7.3 (database UQPY 2023) (Bale *et al.*, 2016) in the slag assuming a stoichiometric reaction as shown in equation *8*).

$$Fe_2O_3 + Fe \rightarrow 3\,FeO \qquad 8)$$

TABLE 1 - Starting composition of the slag for electrical conductivity measurements (in mol%).

	CaO	SiO_2	$AlO_{1.5}$	'FeO'
Mol%	33.55	29.75	16.00	20.70

This mixture was put in an alumina crucible inside a muffle furnace at 1240 °C overnight. This CAS sinter was then added to Fe_2O_3 powder (99.8%) and Fe powder (99.9%). All powders were thoroughly mixed in a pestle and mortar before being pelletized. This powder mixture was then brought into the alumina crucible and put inside the furnace. The advantage of using the CAS sinter compared to the pure powders was that it aided the pelletizing procedure and that it prevented powder ejection/slag foaming due to a release of CO_2 gas at elevated temperatures. After the furnace was completely sealed off from the surrounding atmosphere, it was flushed with the desired gas composition at a flow rate of 1 l/min for 9 hours. The temperature was subsequently increased to 1310 °C at a rate of 5 °C/min and kept for 6h to allow melting of the powder and homogenization of the bath.

The bath surface was then determined in a similar way as for the calibration. However, it was found that the slag wetted the crucible significantly which resulted in the formation of a meniscus as illustrated in FIG - *4*. To take into account this difference in bath geometry between high temperature experiment and low temperature calibration, a correction procedure for the slag meniscus was adopted which is schematically illustrated in the right side of FIG - *4*. The idea is that the displacement sensor readings h_{sensor} upon touching the slag surface for each electrode combination are recorded. Plotting the sensor reading as a function of the electrode positions allowed then to estimate the slag meniscus via a parabolic function to extract the bath surface which was defined as the minimum of the meniscus. The authors are aware that this method is only an approximation of the reality and that this fitting is influenced by the electrode spacing and deviations of the meniscus from a parabolic profile. However, since differences of 1 – 2 mm were found between positions $h_{A,D}$ and $h_{A,B}/h_{A,C}$ it was deemed necessary to estimate the meniscus profile and to correct for the geometry difference at high temperature and calibration.

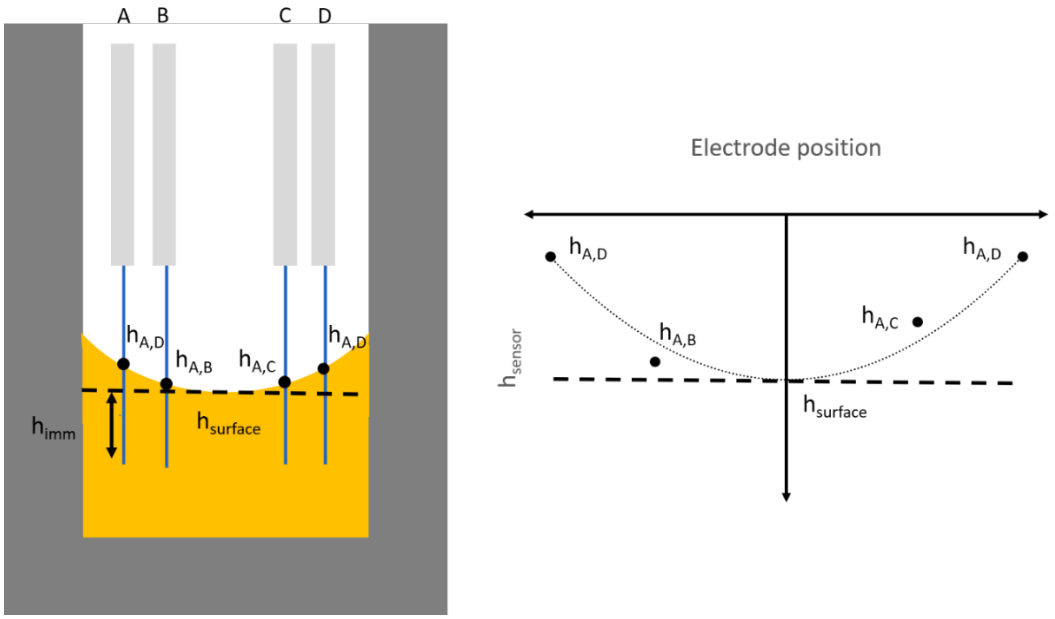

FIG - 4 Schematic illustration of the fitting procedure for determining the bath surface at high temperature experiments.

After determination of the bath surface, the electrodes were lowered to an immersion depth of 10 mm. Similar to the calibration, a frequency sweep was carried out. For the high temperature experiments, the real impedance was frequency-independent over a broad range from 100 Hz to 50 kHz. Single frequency measurements were carried out at 10 kHz at immersion depths of 8, 9, 10, 11 and 12 mm starting with the one at 10 mm. After the single frequency measurements, the electrode configuration was changed to a three-electrode configuration using electrode positions B, C and D for the counter, reference and working electrode, respectively, and the immersion depth was again placed at 10 mm. The open circuit potential of the system was then recorded for 10 minutes after which stepped potential chronoamperometry was executed. The system was held at OCP for 1 minute prior to a voltage step of -10 mV (vs OCP) for 40 minutes during which the current was measured at a scan rate of 100 Hz. Preliminary experiments indicated that positive voltages, applied between working and reference electrode, would result in electrode plating at the counter electrode for low oxygen partial pressures. In addition, a long time for the voltage step was needed as the system progressed slowly to a stable current I_∞. After stepped potential chronoamperometry, the configuration was switched back to the earlier four-electrode setup and single frequency measurements were done at the same immersion depths as before. Comparison of these values allowed to quantify any changes in the electrical conductivity as a result of crucible dissolution into the slag, which could have taken place during the stepped potential chronoamperometry. After this final measurement, the electrodes were lifted outside the slag and the crucible was quenched. The slag was then mounted in epoxy resin for electron probe X-ray microanalysis (EPMA) with wavelength dispersive detectors (JEOL 8200L EPMA, Japan Electron Optics Ltd., Tokyo, Japan). All elements were measured using the conventional EPMA technique. The conventional EPMA measurement was performed with an acceleration voltage of 15 keV, a beam current of 20nA and a probe diameter ranging from 5 to 30 µm depending on the specific phase being analysed. The following detectors and spectral lines were employed for elemental measurement: Al K_α – TAP, Fe K_α – LIF, Si K_α – PET J, Ca K_α – PET J. For the measurement of Al, Fe, Si and Ca cations, pure (synthetic) $AlO_{1.5}$, Fe_2O_3, SiO_2 and $CaSiO_3$ standards were used, respectively, provided by Charles M. Taylor. Raw measured data underwent standard ZAF correction using the Armstrong/Love Scott approach.

Results

The measured compositions of the slag samples using EPMA for different conditions are provided in *TABLE 2*. Both CaO and SiO_2 match the desired target composition, whereas for $AlO_{1.5}$ and 'FeO', there seems to be respectively a 1% increase and decrease. The increase in $AlO_{1.5}$ stems from a continuous dissolution of the crucible into the liquid slag. The decrease in 'FeO' on the other hand might stem from reactions going on between the crucible and the slag at the slag-crucible interface, such as dissolution of hematite ($FeO_{1.5}$) into the alumina crucible and/or the formation of Fe/Al-containing spinels. For p_{O2} values of 10^{-5} atm and $10^{-7.92}$ atm, a spinel layer covering the crucible was indeed observed. For the sample at 10^{-5} atm, an additional loose spinel layer was found up to about 1.57 mm above the crucible bottom where spinels are suspended in the liquid slag. However, it is expected for this layer to have a limited effect on the measurements as there always is around 9 mm – 14 mm of fully liquid slag between the lowest points of the electrodes and the loose layer. Due to this relatively large distance, it is expected that only a minor fraction of the total current reaches this loose spinel layer.

TABLE 2 - Measured slag compositions (mol%) after quenching for different oxygen partial pressures (p_{O2}, log(atm)).

p_{O2}	Fe^{3+}/Fe_{tot}	SiO_2	CaO	$AlO_{1.5}$	'FeO'
-0.67	0.89	29.78 ± 0.18	33.27 ± 0.14	17.46 ± 0.16	19.50 ± 0.11
-5.00	0.51	29.95 ± 0.33	33.24 ± 0.31	17.02 ± 0.48	19.79 ± 0.20
-7.92	0.20	30.02 ± 0.22	33.43 ± 0.18	16.69 ± 0.19	19.80 ± 0.12

The total, electronic and ionic conductivity and the electronic transference number as a function of the predicted Fe^{3+}/Fe_{tot} ratio is given in *FIG - 5* and *FIG - 6*. The experimental reproducibility lies between 3% and 20% for the total electrical conductivity and below 3% on electronic transference numbers. The uncertainty due to crucible dissolution before and after stepped potential

chronoamperometry was below 5% on the total electrical conductivity. This mild effect of crucible dissolution is likely the result of working at near saturation conditions of the slag which was the target of the initial small scale experiments as well as the formation of this protective spinel layer at the slag-crucible boundary (Vergote *et al.*, 2021).

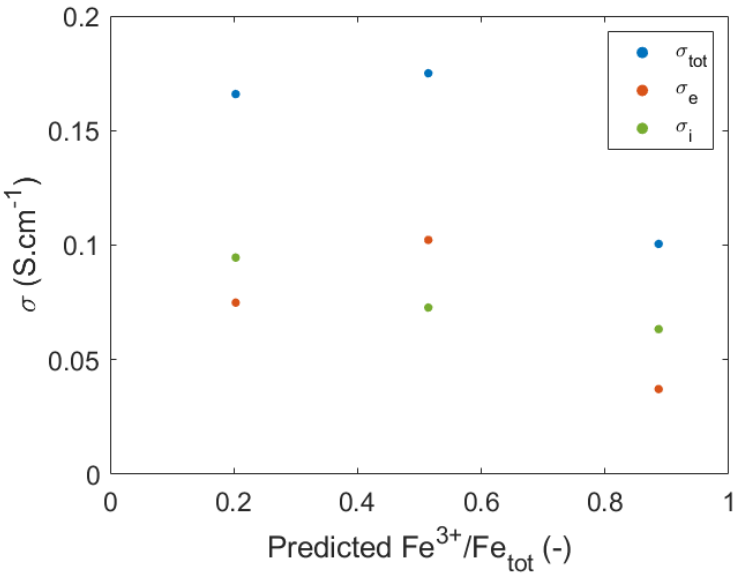

FIG - 5. Total, electronic and ionic conductivity (S/cm) as a function of the predicted Fe^{3+}/Fe_{tot} ratio for the slag.

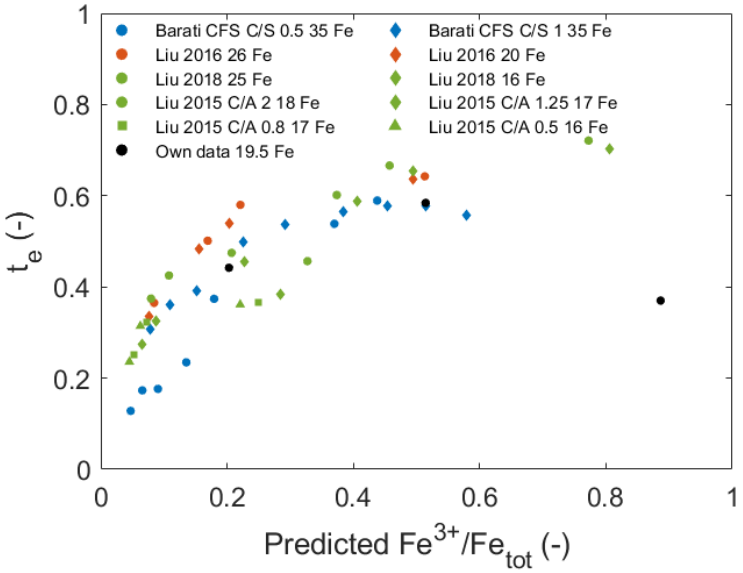

FIG - 6. Electronic transference number as a function of the Fe^{3+}/Fe_{tot} ratio predicted via FactSage UQPY 2023 for our experimental data and data obtained from literature. The amount of Fe cations per 100 mol slag for each study is also included in the figure's legend.

Even from a limited number of experimental conditions, some trends can already be confirmed. First of all, both the total and electronic conductivity seem to exhibit a maximum between the two extremes of a p_{O2} of $10^{-0.67}$ atm and 10^{-8} atm or Fe^{3+}/Fe_{tot} values of 0.89 and 0.20, respectively. This is expected as an equal number of Fe^{2+} and Fe^{3+} provides optimal conditions for electron hopping (Barati and Coley, 2006a, 2006b). Second, the ionic conductivity increases with decreasing Fe^{3+}/Fe_{tot} ratio as the less mobile Fe^{3+} cations are replaced by more mobile Fe^{2+} cations.

Finally, the obtained electronic transference number is compared with several reported literature values (Barati and Coley, 2006a; Liu, Zhang and Chou, 2015; J. H. Liu *et al.*, 2016; Liu *et al.*, 2018). The Fe^{3+}/Fe_{tot} ratios of these other studies are estimated via FactSage UQPY 2023 from the reported slag composition and conditions (gas flow rate, temperature). Since electronic transference numbers are independent of temperature, this value can provide a better means for comparing

electrical conductivity setups/measurements. Moreover, comparison of electronic transference numbers between different slag compositions is roughly possible on the condition that the concentration of the two Fe cations between both slags is of a similar magnitude. From equation *5*), the electronic transference number is the ratio of the electronic conductivity over the sum of the electronic and ionic conductivity. The electronic conductivity, equation *9*), is assumed to depend on the Fe^{2+} diffusion coefficient D_{Fe2+} (cm^2/s), the concentration of Fe cations [Fe] (mol/cm^3) and the Fe^{3+}/Fe_{tot} ratio y (-) (Engell and Vygen, 1968; Barati and Coley, 2006b). The ionic conductivity is typically described via the Nernst-Einstein equation (Thibodeau and Jung, 2016) which assumes that the total ionic conductivity is the sum of the contribution of each cation in the melt as shown in equation *10*) in which z_i is the charge of cation i, F is the Faraday constant, R is the universal gas constant, T is the temperature (K), [i] is the concentration of cation i (mol/cm^3) and D_i its diffusion coefficient (cm^2/s). Therefore, the electronic transference number can be described according to equation *11*). This equation shows that the electronic transference for slags with a similar Fe concentration has a more or less parabolic shape as a function of the Fe^{3+}/Fe_{tot} ratio (y) with the maximum value being shifted according to the ionic conductivity of the other cations in the slag. FIG - *6* shows that the electronic transference number of the current study lies within the expected order of magnitude for slags with a similar 'FeO' content.

$$\sigma_e = C_1 D_{Fe2+} [Fe]^2 y(1-y) \quad 9)$$

$$\sigma_{ion} = \sum_i \frac{{z_i}^2 F^2}{RT} [i] D_i \quad 10)$$

$$t_e = \frac{\sigma_e}{\sigma_e + \sigma_i} = \frac{C_1 D_{Fe2+} [Fe]^2 y(1-y)}{C_1 D_{Fe2+} [Fe]^2 y(1-y) + \frac{4F^2}{RT} D_{Fe2+} (1-y)[Fe] + \sum_{i,i \neq Fe2+} \frac{{z_i}^2 F^2}{RT} [i] D_i} \quad 11)$$

CONCLUSION

The aim of the present study was to validate and obtain a methodology for electrical conductivity measurements on CaO – $AlO_{1.5}$ – SiO_2 – 'FeO' slags for varying oxygen partial pressures in a newly built setup which allows quenching and post-experimental verification of the composition and microstructure. Experiments were carried out in three different atmospheres: air (p_{O2} = 0.21 atm) and two CO_2/CO/Ar gas mixtures with an oxygen partial pressure of 10^{-5} atm and $10^{-7.92}$ atm. The electrical conductivity was found to be stable throughout the experiment due to saturation of the slag with $AlO_{1.5}$ and the formation of protective layer at the slag-crucible interface for some conditions. In addition, microstructural analysis of the samples showed that an unexpected loose spinel layer formed during the experiment at $p_{O2} = 10^{-5}$ atm. Although the effect of this layer was assumed to be negligible, it nonetheless shows the need for post-experimental microstructural analysis to confirm which phases were present during the effective measurement. Overall, the experimental reproducibility of the setup varied between 3% and 20%. From a limited set of conditions, the expected trends were confirmed: an increase in the ionic conductivity from more oxidizing (Fe^{3+} rich) to more reducing (Fe^{2+} rich) conditions. Also, a maximum in the electronic conduction is expected based on the observed peak at the predicted Fe^{3+}/Fe_{tot} ratio of 0.5 within the other two conditions. Finally, it was proven that electronic transference numbers of the current study have a similar order of magnitude as those from earlier studies in literature.

ACKNOWLEDGEMENTS

P.J. Boeykens holds a grant [HBC.2020.2248] which is supported by VLAIO, the Flanders Innovation & Entrepreneurship Agency, in co-operation with Umicore. I. Bellemans holds a grant from the Research Foundation Flanders [1239024N]. The authors would like to express their thanks to R. Starykh for aiding in the construction of the electrical conductivity setup and for EPMA measurements.

REFERENCES

Bale, C.W. *et al.* (2016) 'FactSage thermochemical software and databases, 2010-2016', *Calphad: Computer Coupling of Phase Diagrams and Thermochemistry*, 54, pp. 35–53. Available at: https://doi.org/10.1016/j.calphad.2016.05.002.

Barati, M. and Coley, K.S. (2006a) *Electrical and electronic conductivity of CaO-SiO2-FeO x slags at various oxygen potentials: Part I. Experimental results*, *Metallurgical and Materials Transactions B: Process Metallurgy and Materials Processing Science*. Available at: https://doi.org/10.1007/s11663-006-0084-x.

Barati, M. and Coley, K.S. (2006b) 'Electrical and electronic conductivity of CaO-SiO2-FeO x slags at various oxygen potentials: Part II. Mechanism and a Model of Electronic Conduction', *Metallurgical and Materials Transactions B: Process Metallurgy and Materials Processing Science*, 37(1), pp. 41–49. Available at: https://doi.org/10.1007/s11663-006-0084-x.

Bard, A.J. and Faulkner, L.R. (2001) *ELECTROCHEMICAL METHODS Fundamentals and Applications*. second edi, *Annual Review of Materials Science*. second edi. John Wiley & Sons Inc.

Bellemans, I. *et al.* (2018) 'Metal losses in pyrometallurgical operations - A review', *Advances in Colloid and Interface Science*, 255, pp. 47–63. Available at: https://doi.org/10.1016/j.cis.2017.08.001.

Boeykens, P.-J. *et al.* (2023a) 'Electrical conductivity measurements in PbO-SiO2-FeOx slags', in *EMC 2023*.

Boeykens, P.-J. *et al.* (2023b) 'Parameter investigation of the experimental methodology of electrical conductivity measurements for PbO containing slags', *Electrochimica Acta*, 464, p. 142846. Available at: https://doi.org/10.1016/J.ELECTACTA.2023.142846.

Dalvi, A.D. (2023) 'Decarbonization of Mining and Metals Industry. A Critical Overview', *Proceedings of the 61st Conference of Metallurgists, COM 2022*, 1, pp. 917–937. Available at: https://doi.org/10.1007/978-3-031-17425-4_103.

Engell, H.-J. and Vygen, P. (1968) 'Ionen- und Elektronenleitung in CaO-FeO-Fe2O3-SiO2-Schmelzen', *Berichte der Bunsengesellschaft für physikalische Chemie*, 72(1), pp. 5–12. Available at: https://doi.org/https://doi.org/10.1002/bbpc.19680720104.

Evgueni, J. *et al.* (2022) 'Integrated Experimental Phase Equilibria and Thermodynamic Modelling Research and Implementation in Support of Pyrometallurgical Copper Processing', in *11th International Conference on Copper*. Santiago, Chile: Instituto de Ingenieros de Minas de Chile, pp. 608–634.

Fried, N.A., Rhoads, K.G. and Sadoway, D.R. (2001) 'Transference number measurements of TiO2-BaO melts by stepped-potential chronoamperometry', *Electrochimica Acta*, 46(22), pp. 3351–3358. Available at: https://doi.org/10.1016/S0013-4686(01)00531-X.

Friedrich, B. *et al.* (2018) 'The Submerged Arc Furnace (SAF): State-of-the-Art Metal Recovery from Nonferrous Slags', *Journal of Sustainable Metallurgy*, 4(1), pp. 77–94. Available at: https://doi.org/10.1007/s40831-017-0153-1.

Gruener, G. *et al.* (1998) 'Measurements of conductivity in liquids. Application to 2CaOAl2O3SiO2', *EPJ Applied Physics*, 4(1), pp. 101–106. Available at: https://doi.org/10.1051/epjap:1998248.

Hundermark, R. (2003) 'The electrical conductivity of melter type slags'. University of Cape Town.

Karalis, K.T. *et al.* (2016) 'A CFD analysis of slag properties, electrode shape and immersion depth effects on electric submerged arc furnace heating in ferronickel processing', *Applied Mathematical Modelling*, 40(21), pp. 9052–9066. Available at: https://doi.org/https://doi.org/10.1016/j.apm.2016.05.045.

Liu, Jun Hao *et al.* (2016) 'Electrical Conductivity and Electronic/Ionic Properties of TiOx-CaO-SiO2 Slags at Various Oxygen Potentials and Temperatures', *Metallurgical and*

Materials Transactions B: Process Metallurgy and Materials Processing Science, 47(1), pp. 798–803. Available at: https://doi.org/10.1007/s11663-015-0499-3.
Liu, J. H. *et al.* (2016) 'Study on electrical conductivity of FexO–CaO–SiO2–Al2O3 slags', *Canadian Metallurgical Quarterly*, 55(2), pp. 221–225. Available at: https://doi.org/10.1080/00084433.2016.1150545.
Liu, J.H., Zhang, G.H. and Chou, K.C. (2015) 'Electronic/ionic properties of FexO-SiO2-CaO-Al2O3 slags at various oxygen potentials and temperatures', *ISIJ International*, 55(11), pp. 2325–2331. Available at: https://doi.org/10.2355/isijinternational.ISIJINT-2015-325.
Liu, J.H., Zhang, G.H. and Wang, Z. (2017) 'Experimental Study on Electrical Conductivity of MnO-CaO-SiO2 Slags at 1723 K to 1823 K (1450 °C to 1550 °C) and Various Oxygen Potentials', *Metallurgical and Materials Transactions B: Process Metallurgy and Materials Processing Science*, 48(6), pp. 3359–3363. Available at: https://doi.org/10.1007/s11663-017-1072-z.
Liu, Y.X. *et al.* (2018) 'Experimental Study on Electrical Conductivity of FexO-CaO-SiO2-Al2O3 System at Various Oxygen Potentials', *High Temperature Materials and Processes*, 37(2), pp. 121–125. Available at: https://doi.org/10.1515/htmp-2016-0102.
Martin-Treceno, S. *et al.* (2022) 'Determination of the Partial Contributions to the Electrical Conductivity of TiO2-SiO2-Al2O3-MgO-CaO Slags: Role of the Experimental Processing Conditions', *Metallurgical and Materials Transactions B: Process Metallurgy and Materials Processing Science*, 53(2), pp. 798–806. Available at: https://doi.org/10.1007/S11663-022-02433-5/FIGURES/7.
Mills, K.C. *et al.* (2013) 'The Structure and Properties of Silicate Slags', in *Treatise on Process Metallurgy*. Elsevier Ltd., pp. 149–286. Available at: https://doi.org/10.1016/B978-0-08-096986-2.00008-4.
Pomeroy, M. *et al.* (2012) 'Comparison of the electronic conduction mechanism in MnO x-CaO-SiO 2 and FeO x-CaO-SiO 2 slag systems', *High Temperature Materials and Processes*, 31(3), pp. 231–236. Available at: https://doi.org/10.1515/htmp-2012-0042.
Schiefelbein, S.L. *et al.* (1998) 'A high-accuracy, calibration-free technique for measuring the electrical conductivity of liquids', *Review of Scientific Instruments*, 69(9), pp. 3308–3313. Available at: https://doi.org/10.1063/1.1149095.
Schupsky, J.P. *et al.* (2020) 'The Impact of Sample Homogeneity, Crucible Material, and Oxygen Partial Pressure on the Crystallization of Fe-Rich Oxidic Slag in CLSM Experiments', *Journal of Sustainable Metallurgy*, 6(2), pp. 216–226. Available at: https://doi.org/10.1007/S40831-020-00262-X/TABLES/2.
Thibodeau, E., Gheribi, A.E. and Jung, I.H. (2016a) 'A Structural Molar Volume Model for Oxide Melts Part I: Li2O-Na2O-K2O-MgO-CaO-MnO-PbO-Al2O3-SiO2 Melts—Binary Systems', *Metallurgical and Materials Transactions B: Process Metallurgy and Materials Processing Science*, 47(2), pp. 1147–1164. Available at: https://doi.org/10.1007/s11663-015-0548-y.
Thibodeau, E., Gheribi, A.E. and Jung, I.H. (2016b) 'A Structural Molar Volume Model for Oxide Melts Part II: Li2O-Na2O-K2O-MgO-CaO-MnO-PbO-Al2O3-SiO2 Melts—Ternary and Multicomponent Systems', *Metallurgical and Materials Transactions B: Process Metallurgy and Materials Processing Science*, 47(2), pp. 1165–1186. Available at: https://doi.org/10.1007/s11663-015-0543-3.
Thibodeau, E., Gheribi, A.E. and Jung, I.H. (2016c) 'A Structural Molar Volume Model for Oxide Melts Part III: Fe Oxide-Containing Melts', *Metallurgical and Materials Transactions B: Process Metallurgy and Materials Processing Science*, 47(2), pp. 1187–1202. Available at: https://doi.org/10.1007/s11663-015-0549-x.
Thibodeau, E. and Jung, I.H. (2016) 'A Structural Electrical Conductivity Model for Oxide Melts', *Metallurgical and Materials Transactions B: Process Metallurgy and Materials*

Processing Science, 47(1), pp. 355–383. Available at: https://doi.org/10.1007/s11663-015-0458-z.
Vergote, O. *et al.* (2021) ‘Towards More Reliable $${\text{ {PbO}-{SiO}}}_{2}$$Based Slag Viscosity Measurements in Alumina via a Dense Intermediate Spinel Layer’, *Metallurgical and Materials Transactions B*, 52(6), pp. 3646–3659. Available at: https://doi.org/10.1007/s11663-021-02328-x.
Zhao, B. *et al.* (2009) ‘Viscosity and electrical conductivity of copper slag at controlled oxygen potential’, in *Molten 2009: Proceedings of the VIII International Conference on Molten Slages, Fluxes and Salt*, pp. 225–235.